

UV curing study of semi-dense asphalt mixes with different sizes of copper slag – A sustainable rehabilitation and production strategy

Andrea Rojas-Pardo^a, Osvaldo Muñoz-Cáceres^{a, b, *}, Aitor C. Raposeiras^{a, c},
Diana Movilla-Quesada^{a, d}, Daniel Castro-Fresno^b

^a Gi²V Transportation Engineering Research Group, Institute of Civil Engineering, Faculty of Engineering Sciences, Universidad Austral de Chile, General Lagos St., #2060, Valdivia 5090000, Chile

^b GITECO Research Group, Department of Transportation and Technology of Projects and Processes, Universidad de Cantabria, Av. Los Castros s/n, Santander 39005, Spain

^c Departamento de Ingeniería Mecánica, Escuela Politécnica Superior de Zamora, Universidad de Salamanca, Zamora, España

^d Departamento de Construcción y Agronomía, Escuela Politécnica Superior de Zamora, Universidad de Salamanca, Av. Requejo #33, Zamora 49022, Spain

ARTICLE INFO

Keywords:

Self-healing
Copper slag
Viscosity
Temperature
UV radiation

ABSTRACT

The environmental and service conditions exposed to asphalt pavements affect their rheological and performance properties, making them brittle material susceptible to cracking. One way to partially re-establish the mechanical properties of the cracked pavements is through binder runoff through the cracks in a capillary healing process. It is possible to incorporate conductive materials (electrical or thermal) in asphalt mixtures as additives or partial substitutes for the natural aggregate to maximize the efficiency of the self-healing process and induce a pseudo-Newtonian flow behavior in the binder. The present study evaluated the self-healing performance by UV radiation of asphalt mixtures incorporating copper slag (CS) in different sizes (2.00 mm, 0.25 mm, < 0.063 mm) as a conductive material (heat diffuser) in partial replacement of the natural aggregate. Likewise, the degree of ageing caused by the self-healing process was evaluated through the rheological characterization of the binder extracted after healing. All the CS mixes obtained self-healing rates in mechanical strength higher than 40 %, in particular, the 2.00 mm CS mixes with self-healing rates close to 60 %. The optimum self-healing temperatures for mixtures with CS sizes with higher thermal inertia are between 95 °C and 105 °C corresponding to 18000 s and 30000 s of healing, while for mixtures with CS sizes with lower thermal inertia the optimum self-healing temperatures are between 105° and 110°C corresponding to self-healing times of 18000 s to 25000 s. It was not possible to determine an accelerated ageing effect in the asphalt mixtures due to the self-healing processes by UV radiation.

1. Introduction

The asphalt mix is a material that is mainly composed of a mineral structure made up of aggregates of different sizes (coarse and fine), a binder or asphalt agglomerate, and possibly additives. Its function is to provide pavements with a comfortable, safe, and resistant running surface, facilitating vehicular flow [1]. However, these properties can be affected due to environmental conditions and repeated traffic stresses or loads to which the pavements are subjected in service conditions [2, 3].

The exposure of asphalt mixes to environmental conditions of humidity and temperature variations affects not only the adhesiveness

and cohesion of the bituminous mastic (mixture of filler and binder) but also generates oxidation of the asphalt binder, increasing its rigidity, aging it, and turning it into a brittle material susceptible to cracking [4–7]. On the other hand, the frequent intensification of axle loads coupled with the continuous action of traffic loads favors the appearance and propagation of cracks [8,9]. These cracks generally originate from the base layer in the form of micro-cracks and propagate towards the surface or wearing course in the form of cracks, gradually increasing in length and thickness [10,11]. This phenomenon reduces the load-bearing capacity of pavements and favors the harmful action of external agents, in particular damage caused by moisture, allowing surface water to penetrate the mix, reducing the service life of the pavement.

* Corresponding author at: Gi²V Transportation Engineering Research Group, Institute of Civil Engineering, Faculty of Engineering Sciences, Universidad Austral de Chile, General Lagos St., #2060, Valdivia 5090000, Chile.

E-mail addresses: andrea.rojas.pardo@uach.cl (A. Rojas-Pardo), osvaldo.munoz@uach.cl (O. Muñoz-Cáceres), aitor.raposeiras@uach.cl (A.C. Raposeiras), dmovilla@usal.es (D. Movilla-Quesada), castrod@unican.es (D. Castro-Fresno).

<https://doi.org/10.1016/j.conbuildmat.2022.128621>

Received 6 December 2021; Received in revised form 8 May 2022; Accepted 27 July 2022
0950-0618/© 20XX

Several authors have proposed to extend the service life of pavements by recovering their mechanical properties after a process called “self-healing” [12–15]. This process consists of sealing the micro-cracks and fissures in cracked asphalt pavements through a binder flowing through the crack and the application of an energy source (heat or electricity) [16–18] or the targeted incorporation of rejuvenating additives [19]. The asphalt binder exhibits viscoelastic behavior, which is dependent on temperature, frequency, and intensity of loading. Depending on the temperature, it starts to behave like a Newtonian fluid at temperatures ranging from 30 °C to 70 °C. Above these temperatures, the binder can start to flow (Newtonian flow) through open cracks in the pavement in a kind of capillary flow [20–23].

It is possible to incorporate rejuvenating additives or electrically or thermally conductive materials as additives or partial substitutes for the aggregate to induce self-healing in asphalt mixtures. The selection of the type of material to be used will depend on the planned self-healing method.

The main self-healing methods studied so far differ from each other in the way they modify the binder viscosity of the cracked mixture.

Self-healing by capsules is fundamentally based on the restitution of the liquid phase of the binder by applying a localized rejuvenating additive on the cracked area. For this purpose, microcapsules filled with rejuvenating additives (oils, salts, and sands) are incorporated in the manufacturing process of the asphalt mix [24–26]. When a crack appears in the capsule area, it will break, releasing the rejuvenating additive, which will wet the surrounding bituminous binder, modifying its viscosity and flowing through the crack [16,19].

On the other hand, induction, microwave, and infrared or ultraviolet (UV) self-healing methods seek to modify the flow behavior of the binder after a localized or global increase in the temperature of the mixture.

Induction heating requires the incorporation of a magnetic and conductive material (whether electrical or thermal) in the mixture for its operation. These conductive materials are mainly fillers and metallic fibers [16,27], and they will form a closed circuit around the crack to which an alternating current is induced by applying an electromagnetic field. The heat generated through the energy dissipated by the resistance of the conductive material increases the localized temperature of the mixture, modifying the flow behavior of the binder [28].

Another alternative is microwave self-healing, which increases the overall temperature of the asphalt mixture by microwave radiation, causing the polar molecules to change their orientation due to the generated alternating magnetic field. This effect causes an increase in the temperature of the material by internal friction [29]. The addition of ferrous particles reflects the microwave radiation, accelerating the temperature increase in the mixture [30–32].

Finally, self-healing by infrared or UV radiation is fundamentally based on increasing the temperature of the mixture by the absorption of incident electromagnetic waves with different wavelengths (from 0.7 μm for infrared to 400 nm for UV light), which are then converted into thermal energy by the receiving body. The radiation to which the mixture is subjected increases the kinetic energy (internal energy) of the atoms present, facilitating their movement and interaction and transmitting this energy in the form of heat to the adjacent particles [33].

One of the main advantages of these self-healing methodologies compared to capsule self-healing is that they allow several self-healing processes independent of the magnitude of the damage caused. Within this context, the incorporation of materials that maximize self-healing by UV light seems to be the most sustainable alternative from an environmental and technical point of view due to the complement that can be achieved with the temperature increase by solar radiation in summer periods [34].

The use of copper slag (CS), an industrial by-product waste obtained from the pyrometallurgical production of copper, could contribute to the self-healing of asphalt mixes because it has lower thermal inertia

than aggregate [35] and its use has been studied previously in the mechanical performance of asphalt mixes with good results (see Table 1). On the other hand, the copper mining industry is Chile's main economic contributor, generating a large amount of solid waste that is deposited in landfills, causing a significant environmental impact. It is estimated that the country produces around 5.9 million tons of refined copper with a production of more than 13 million tons of copper slag per year, so its reuse and valorization is a matter of interest [36].

The present study evaluated the self-curing performance of UV asphalt mixes incorporating CS in different sizes (2.00 mm, 0.25 mm, < 0.063 mm) in partial replacement of natural aggregate. These mixes were compared with the performance shown by a conventional mix without the addition of CS under different self-healing periods, i.e., 10800 s to 32400 s. In addition, a rheological study of the binder properties after the most severe manufacturing and self-healing process (32400 s) was carried out and compared with the rheological properties of the virgin binder, to determine the degree of aging of the self-healing process.

2. Materials and methods

In this research, 68 test samples were designed and divided into four different asphalt mixtures (MR, M1, M2, M3). These mixes differ by the partial substitution of different sizes of natural aggregate (AG) by copper slag (CS). The MR mix corresponds to a reference mix without the addition of CS.

2.1. Aggregates and binder

The natural aggregate (AG) used in the manufacture of the asphalt mixes is ophite for the coarse aggregate and limestone for the fine aggregate and filler. These aggregates come from a local quarry located in the city of Santander (Spain). The dosage of the different mixes designed was adjusted and combined to the center of the spindle of the semi-dense “AC16S” granulometric band specified in the European standard for bituminous mixes EN 13108-1 and the Spanish standard “General Technical Requirements for Works of Roads and Bridges” (PG-3). This granulometry is mainly used in wearing courses for newly constructed pavements or as pavement reinforcement for any type of traffic.

Asphalt binders are generally classified according to their degree of penetration or viscosity or their PG grade [39]. Asphalt binder is an adhesive and hydrophobic material, highly viscous in character and at room temperature more or less solid [40]. The main component of the asphalt binder is bitumen, an organic material derived from petroleum,

Table 1
Previous experiences in mechanical and functional results of CS mixtures.

CS content range (% by volume)	Test	Maximum and minimum results obtained within the CS range used	Reference
3.0–16.5	Water absorption (%)	4.44–1.77	[35]
	ITSR (%)	90–80	
15.0–35.0	Marshall stability (kN)	15–14	[37]
	Resilient modulus (MPa)	7000–6000	
7.5–15.0	Mean texture depth (mm)	0.842–0.666	[38]
	Fatigue, 300 $\mu\text{m}/\text{m}$ (cycles)	7.7×10^5 – 4.7×10^5	
	Ruth Depth, 50 °C (mm)	4.615–3.014	

which is susceptible to aging and temperature variations [41,42]. The asphalt binder used in this research corresponds to a conventional type B50/70 binder, specified in EN 12591.

Table 2 shows the specifications and characteristics of the binder and aggregates used.

2.2. Copper slag

The copper slag (CS) used belongs to a copper extraction mine in central Chile. It corresponds to a type of refrigerated slag (air-cooled) giving rise to slag with glassy characteristics and low water absorption. Its appearance is black, with a smooth or porous texture [35,38]. The CS sizes 2.00 mm and 0.25 mm used in this study (Fig. 1a and b) are natural sizes from landfills, while the CS filler (Fig. 1c) was obtained mechanically to determine the influence of the specific surface area of the conductive material on the self-healing of asphalt mixtures. Table 3 shows the properties of the CS used in this study.

2.3. Materials dosage

The dosage of the materials for the manufacture of the mixes and the partial replacement of the AG by CS was carried out by the weight of the material, due to the similarity in the densities of these materials (2.794 g/cm³ for coarse AG, 2.724 g/cm³ for fine AG and 2.768 g/cm³ for CS). The binder content used was set at 5.0 % of the total mass of the mix to obtain a void content close to 5.0 % for all the samples studied. Table 4 shows the granulometry of the mixes used in the study.

2.4. Experimental development

The experimental stage consists of determining the rate or degree of self-healing of semi-dense asphalt mixes by assessing the strength retained after a UV light heating process (self-healing) of asphalt mixes

Table 2
Properties of the B50/70 binder and aggregates used.

Properties	Standards	Result
<i>Binder B50/70</i>		
Penetration (0.1 mm)	EN 1426	57
Softening Point R&B (°C)	EN 1427	51.6
Frass Point (°C)	EN 12593	-13
Penetration Index	EN 12591	-0.50
Density (g/cm ³)	EN 15326	1.035
Laboratory preparation temperature (°C)	EN 12697-35	150-170
<i>Coarse aggregate</i>		
Density (g/cm ³)	EN 1097-6	2.794
Water absorption (%)	EN 1097-6	0.60
Los Angeles (%)	EN 1097-2	15
Flakiness index (%)	EN 933-3	12
<i>Fine aggregate</i>		
Density (g/cm ³)	EN 1097-6	2.724
Sand equivalent	EN 933-8	78

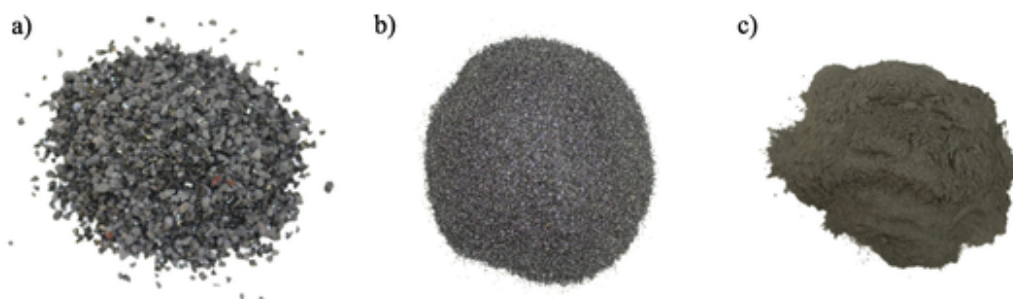


Fig. 1. Sizes of copper slag (CS) used: (a) CS 2.00 mm; (b) CS 0.25 mm; (c) CS Filler (<0.063 mm).

that are previously subjected to a 3-point bending rupture process. Fig. 2 shows a scheme of the experimental development used.

2.4.1. Mix design and preparation

To determine the influence of the conductive particle size (see Fig. 1) on the self-healing rate of semi-dense asphalt mixtures, the design of the asphalt mixtures was carried out by keeping the CS content fixed at 5.0 % AG replacement. This methodology has been used in previous studies and corresponds to the lower percentage of natural aggregate used in the substituted sizes in the reference mix [43]. Table 5 shows the different mixes designed in the study.

The fabrication of the 101.6 mm diameter and 63 mm height study samples was performed following Marshall methodology and EN 12697-35. Before the mixing process, the different fractions of AG and CS separated by size were conditioned at 170 °C for six hours, while the binder was conditioned for two hours at 150 °C. The mixing process was carried out using an automatic laboratory mixer at a temperature of 150 °C according to the specifications of the binder used (Table 2). Finally, the samples were compacted as specified in EN 12697-30 by applying 75 blows per side to later be removed from the mold when they reached room temperature (25 ± 2 °C).

2.4.2. Density and voids

To determine the density of the samples, procedure B: Bulk density – Saturated Surface Dry (SSD) described in EN 12697-6 was used. This density is obtained from Eq. (1).

$$\rho = \frac{m_1}{m_3 - m_2} \cdot \rho_w \quad (1)$$

Where ρ is the bulk density of the sample (g/cm³), m_1 is the mass of the dry specimen (g), m_2 is the mass of the saturated specimen, m_3 corresponds to the mass of the saturated specimen with the dry surface (g) and ρ_w is the density of water at the test temperature (g/cm³).

The void content of the mix is obtained from EN 12697-8. All samples shall comply with article 542 of PG-3 for semi-heavy mixes of type AC16S which corresponds to avoid content between 4 and 6 %.

2.4.3. Three-point bending strength

Previous to the 3-point bending strength test, all specimens were conditioned at a temperature of -20 °C for at least 24 h. This guarantees a clean crack and brittle fracture (without plastic deformation) at the time of breakage. Likewise, before the freezing process, a 0.35 mm wide and 10 mm deep notch was made in the center of the specimen to induce failure in the test specimen and facilitate the breaking procedure (see Fig. 3a).

The 3-point bending strength test consists of determining the maximum ultimate load that a specimen subjected to bending stresses can withstand under the application of an increasing load at a controlled strain rate of 5.0 mm/min at the center of the specimen. The test is terminated by a crack running vertically through the specimen, which coincides with the maximum load-carrying capacity of the specimen due

Table 3
Properties of CS.

Properties	Result	Composition (Oxide)	Result
Density (g/cm ³)	2.768	Fe ₂ O ₃	68.85
Water absorption (%)	1.17	SiO ₂	19.08
Los Angeles (%)	15.54	Al ₂ O ₃	2.59
Crushed particles (%)	89.21	ZnO	2.26
Mohs scale	4-6	CaO	2.07
		CuO	1.08
		Other	<1.0

Table 4
Particle size distribution of the mixes.

Fraction (mm)	MR (%)	M1 (%)	M2 (%)	M3 (%)	AC16-S (%)
22	100.0	100.0	100.0	100.0	100-100
16	95.0	95.0	95.0	95.0	90-100
8	68.0	68.0	67.0	66.0	60-75
4	43.0	43.0	47.0	44.0	35-50
2	32.6	32.6	37.6	34.6	24-38
0.5	13.6	13.6	18.6	14.2	11-21
0.25	9.0	9.0	9.0	9.2	7-15
0.063	5.1	5.1	5.1	5.0	3-7
% Binder*	5.0	5.0	5.0	5.0	>4

* % corresponding to the total mass of the mix.

to the brittleness conditions imposed by the conditioning of the specimens (-20 °C). This methodology is similar to that described in EN 12697-44 (semicircular specimen bending, SCB). The Marshall specimen was used as extracted from fabrication, except for the notch in the center for the simplicity of the method, considering the requirements of the aforementioned standard regarding the distance between the supports and the crack validation zone (± 15 mm from the load center). Fig. 3a shows the loading configuration of the 3-point bending strength test. It should be noted that this test geometry has already been used in previous investigations [44].

After completion of the 3-point bending test, the specimens are conditioned at room temperature (25 ± 2 °C) for 24 h to eliminate the presence of moisture on the failure surface before the self-bonding process (see Fig. 3b).

2.4.4. UV radiation healing

A system of UV radiation bulbs is used to simulate the heating of the samples by solar energy for the self-healing process of the asphalt mixtures model U VITALX 300 WE, radiated power UVA of 13.6 W, UVB of 3.0 W, beam angle of 30°, and 300 W of wattage. For this purpose, the two-sample halves (Fig. 3b) obtained in the bending strength test were firmly joined together with the use of adhesive tape to simulate the lateral confinement of the cracked pavement section. Each test specimen is placed in a container of white sand, exposing only the top side of the specimen to UV radiation to prevent lateral self-healing of the specimen. Twenty test samples were used to adjust three pre-curing parameters before the self-healing process: curing times, bulb height, and environmental conditions.

Each sample is placed under a radiation coil that is placed 20 cm from its upper side, homogenizing the thermal energy delivered to each sample. Subsequently, the different asphalt mix samples are cured for 4 different times, corresponding to $t_1 = 10800$ s, $t_2 = 18000$ s, $t_3 = 25200$ s, and $t_4 = 32400$ s, to obtain temperatures above the softening point of the binder.

The surface temperature of the samples was monitored and recorded using an Optris PI 640i infrared camera with 640×480 Px resolution and a temperature range of -20 °C to 900 °C at the end of each self-healing period.

The test samples are allowed to cool at room temperature (25 ± 2 °C) for 24 h after the self-healing time, and then subjected to a further freezing and breaking process at -20 °C according to section 2.4.3. Fig. 4 shows the self-healing process by UV radiation bulbs.

2.4.5. Self-healing rate

The rate or degree of self-healing of the designed mixtures was determined by obtaining the retained strength ratio of the specimens tested in flexure. This strength ratio ($S(\tau)$) is obtained from the assessment of the three-point flexural strength at break ($F_f(\tau)$) on specimens

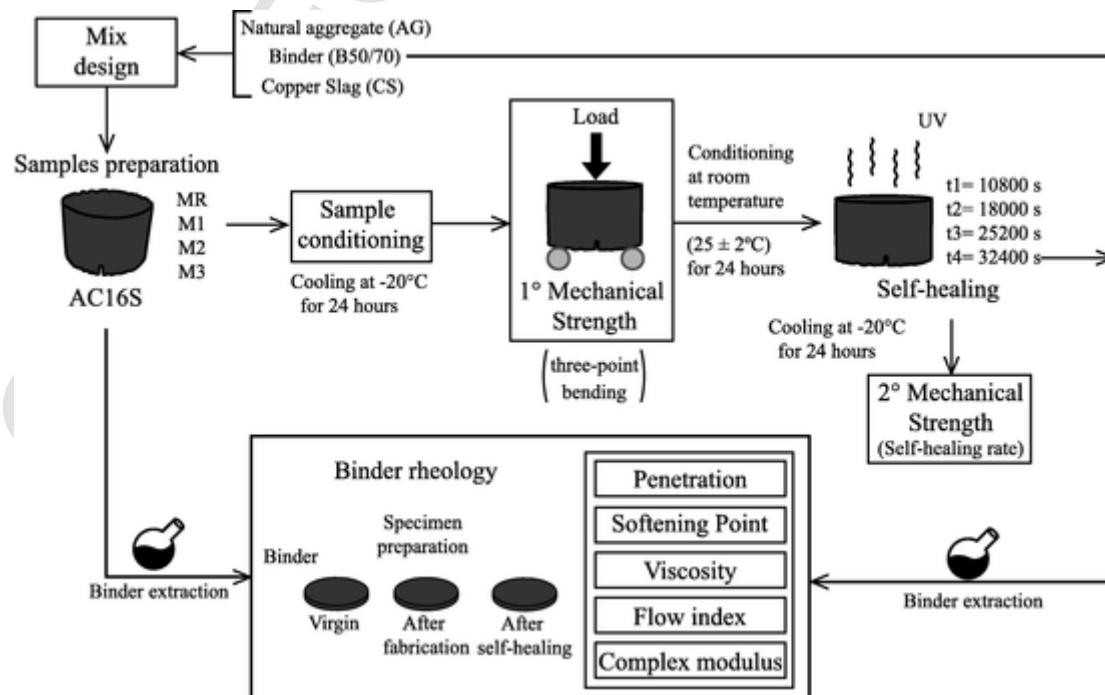


Fig. 2. Experimental study methodology.

Table 5
Mixes developed in the studio.

Mix	CS content (%)	AG size replaced (mm)
MR	0	–
M1	5	2.00
M2	5	0.25
M3	5	<0.063 (Filler)

that have been previously tested at break and that have undergone a self-healing process to reestablish their mechanical properties. The flexural strength of the first rupture of the specimens recorded as (F_i) represents damage to the mix associated with a total loss of its strength capacity. Eq. (2) shows the strength ratio used in the study.

$$S(\tau) = \frac{F_f(\tau)}{F_i} \tag{2}$$

2.4.6. Binder rheology

Rheological characterization tests were performed on the virgin binder and after the fabrication and self-healing processes since the increase of temperature in the self-healing process of asphalt mixtures could induce accelerated aging of the asphalt binder and reduce the effectiveness of subsequent self-healing processes. The tests selected to determine the changes in the rheological properties of the binder are the DSR, penetration, and ring and ball tests. For this purpose, 12 binder samples were recovered through a rotary evaporator from cylindrical samples exposed to manufacturing and self-bathing processes for 32400 s. The combined effect of UV light and UV-rays on the rheological properties of the binder was evaluated. The combined effect of UV light and temperature could cause a higher binder aging than when considering only the effects caused by temperature, better simulating real aging under service conditions [45].

The DSR test was used to determine the complex modulus (G^*) and complex viscosity (η^*) of the recovered and virgin asphalt binder using a dynamic shear rheometer (DSR) at different temperatures and loading frequencies according to EN 14770. A 25 mm diameter parallel plate

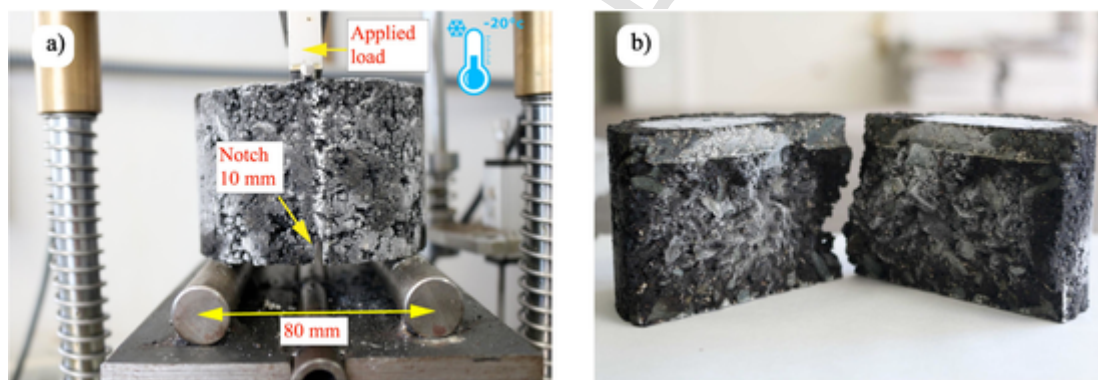


Fig. 3. (a) Pre-conditioning and three-point bending test configuration; (b) Fragile breakage and conditioning at room temperature.

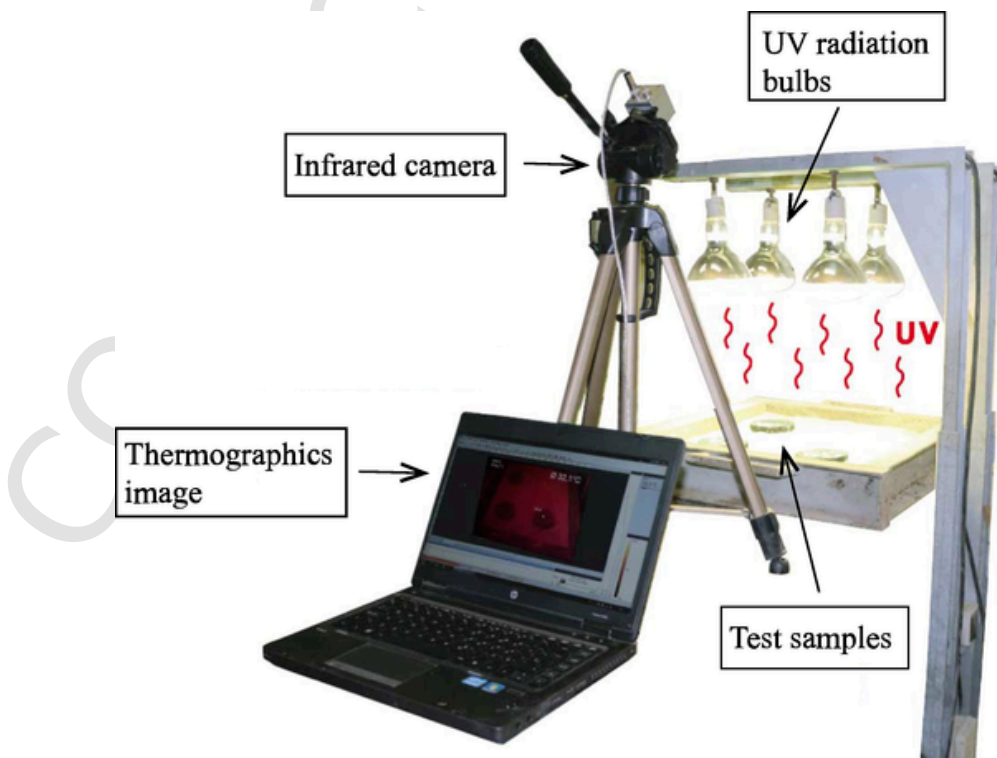


Fig. 4. Self-healing process by UV radiation.

configuration with a 1.0 mm plate spacing was used for this test. The oscillating frequency sweep considered a range of 0.1 to 30 Hz at temperatures between 30 °C and 120 °C (with 10 °C intervals) under the constant strain of 0.1 % deformation. The complex viscosity (η^*) obtained in this test was also used to determine the flow behavior index (n) of the asphalt binder. This dimensionless value determines the deviation from Newtonian behavior of the binder at different temperatures by analytical interpolation of the data obtained and the power function shown in Eq. (3).

$$\eta^* = m \cdot |\omega|^{n-1} \quad (3)$$

where ω is the frequency, η^* is the complex viscosity and m , n interpolation coefficients, with n as the index of flow behavior.

The variation in the high temperature softening point of binders extracted after fabrication and self-healing at 32400 s was determined by the ring and ball test. This method applies to binders with softening points between 28 °C and 150 °C and is carried out according to EN 1427. A distilled water bath was used for this test, discarding test samples where the temperature increase of the water bath was found to be outside 4.4 and 5.6 °C for each minute of testing. Similarly, results were discarded if the difference between the two softening temperatures of the samples where the balls touch the bottom plate is >1 °C.

The consistency of the binders at service temperatures was determined by the needle penetration test described in EN 1426. This test consists of determining the depth, in tenths of a millimeter, reached by a standard needle penetrating vertically into a binder sample under controlled conditions of temperature, load, and duration of load application. The test was carried out at 25 ± 5 °C temperature, applying a load of 100 g for 5 s. Three penetration tests were performed for each type of sample, discarding those results where the difference in the penetration value of the individual samples was greater than 2 tenths of a millimeter.

2.4.7. Statistical analysis

Statistical tests to contrast hypotheses between the different study groups were carried out to analytically determine the significance of the results obtained and to avoid interpretation errors given the dispersion of the experimental data. The results of normality and homoscedasticity of the samples were contrasted using the Shapiro-Wilk test and Levene test, respectively, to determine the statistical tests to be performed.

The parametric test used in the case of samples conforming to a normal distribution is the one-factor ANOVA and the Fisher-Snedecor F-statistic. In the post hoc analysis, Turkey tests and the Games-Howell test for equality of variances were used. For data not following a normal distribution, the non-parametric Kruskal-Wallis H-test and Mann-Whitney U test were used.

In this study, a significance level of 95 % was considered for all tests in the hypothesis test.

3. Results and discussion

3.1. Density and voids

Table 6 shows the values of bulk density and void content for the different mixes designed in this study. According to the results obtained, we can observe that the mean density for all the mixtures manufactured corresponds to 2.442 ± 0.027 g/cm³. No significant differences are observed between the density means for the MR, M1, and M2 mixes with significance values of sig. = 0.463 between MR and M1 and sig. = 0.684 between MR and M3 mixes. However, the M2 mixture generates a significant increase (sig. <0.021) of 1.35 % in its density value concerning the reference mixture and 1.74 % concerning the M1 mixture. This increase in the density of mix M2 translates into a significant decrease (sig. <0.008) in void content, with a

Table 6
Mixtures and design parameters.

Mixture	Self-healing time	Bulk density (g/cm ³)	Mean density (g/cm ³)	Air voids in mixture (%)	Mean of air voids (%)
MR	t_1	2.424	2.434	5.09	4.66
	t_2	2.430		4.85	
	t_3	2.436		4.62	
	t_4	2.447		4.21	
M1	t_1	2.425	2.424	5.58	5.64
	t_2	2.433		5.28	
	t_3	2.415		5.97	
	t_4	2.421		5.72	
M2	t_1	2.468	2.467	4.00	4.04
	t_2	2.467		4.04	
	t_3	2.467		4.02	
	t_4	2.466		4.08	
M3	t_1	2.444	2.442	5.16	5.12
	t_2	2.425		5.76	
	t_3	2.437		5.29	
	t_4	2.463		4.28	

decrease of more than 13.30 % concerning the rest of the mixes. This difference may be due to the fact that mix M2 has a higher content of intermediate sizes from 0.25 mm to 4.0 mm (see Table 4), close to the upper limit of the gradation, filling to a greater extent the voids generated by the larger aggregates. On the other hand, the mixes incorporating CS tend to increase the void content concerning the MR mix (except for the M2 mix), with values higher than 5.00 %; this may be due to the fact that CS has a greater number of fractures faces and a surface with a greater number and pronunciation of voids, cavities, and pores than the surface of conventional aggregates [46,47]. Despite the significant reduction in voids content of the M2 mix, all mixes comply with the voids percentage for wearing courses of 4–6 %.

3.2. Three-point bending strength

The maximum ultimate loads obtained for the different mixes in the three-point bending strength test are shown in Fig. 5. All mixes incorporating CS by AG present a similar behavior to the reference mix in terms of their bending strength, in particular, mix M2 with a <4.0 % de-

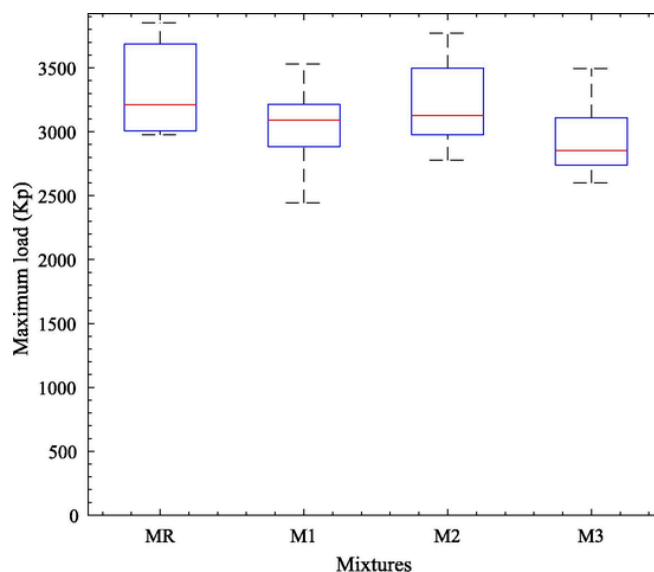


Fig. 5. Results of the maximum three-point bending ultimate load.

crease in its maximum bending load. Mixture M3 presented the lowest flexural strength, with a decrease of 12.26 % compared to the reference mix. This decrease in the flexural strength of the M3 mixes may be due to the fact that the CS filler generates a greater stiffening of the bituminous mastic compared to the limestone filler used in the reference mix, accentuating the brittleness obtained in the mixes under the $-20\text{ }^{\circ}\text{C}$ breaking condition. The highest strengths were found in the mixes with a lower void content, since these samples have a better distribution of stress concentration within the mix (greater contact between the aggregate particles) [48].

3.3. Self-healing rates and healing temperatures

Fig. 6 shows the final temperature reached by the samples as a function of the different healing times. The MR and M1 mixtures presented a higher slope in their temperature curve compared to the M2 and M3 mixes for the lowest self-heating times, reaching differences of up to $18\text{ }^{\circ}\text{C}$ between the mixes with the highest and lowest temperature record. This behavior may be due to smaller CS sizes having higher thermal inertia compared to AG, a phenomenon that decreases when increasing CS particle size.

The mixtures with lower thermal inertia (MR and M1) reached their steady-state temperature (horizontal slope) at approximately 30000 s, with temperatures of $110.7\text{ }^{\circ}\text{C}$ and $108.8\text{ }^{\circ}\text{C}$, respectively. Mixtures M2 and M3 did not show temperature stabilization, with increasing values at all times considered, reaching a maximum temperature of $120.4\text{ }^{\circ}\text{C}$ for mixture M3.

Fig. 7 shows the results obtained in the self-healing rate for the different mixtures designed in the study as a function of the temperature reached in the healing process. Although it is not possible to determine a clear trend in the self-healing rates due to the variability of the data obtained, most of the samples present a healing rate higher than 30 % with an approximate maximum limit of 70 % in the value of the retained strength ($S(\tau)$). Self-healing rates higher than 50 % are obtained for temperatures between $95\text{ }^{\circ}\text{C}$ and $110\text{ }^{\circ}\text{C}$ for all the mixtures, being the optimal temperatures in the self-healing processes. Drops of up to 93.62 % in self-healing rates are observed when $110\text{ }^{\circ}\text{C}$ is exceeded in the healing process, which is a limiting temperature for healing. An excessive decrease in binder viscosity generates a lower surface tension between the binder, the crack walls, and the aggregates, causing an overflow of the binder from the top to the bottom of the sample. This healing phenomenon would reopen the cracks and modify the distribution and void content in the specimen, decreasing the self-healing rates and the strength of the material [20,33].

The highest values in self-healing rates for the mixtures with lower thermal inertia, i.e., the MR and M1 mixtures, are reached at higher

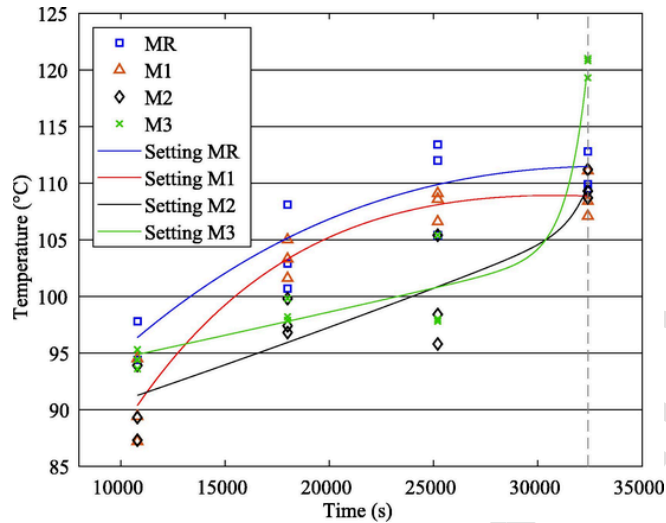


Fig. 6. The maximum surface temperature of the samples at different healing times.

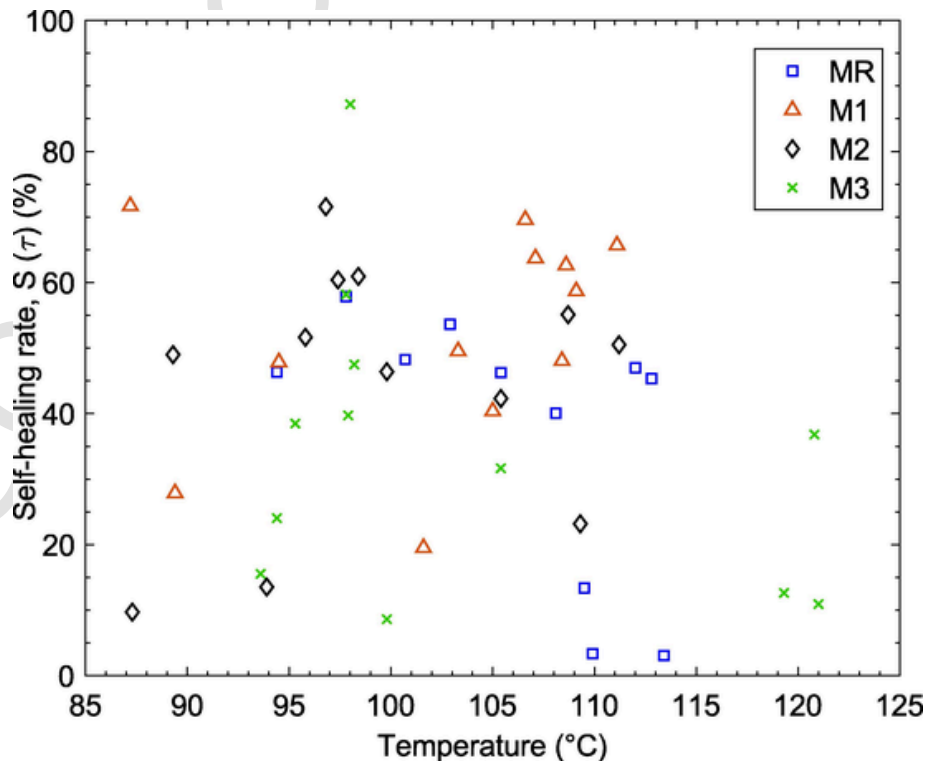


Fig. 7. Self-healing rate using the conserved strength ratio $S(\tau)$ at different temperatures.

temperatures (upper limit of the optimum range, 105 °C-110 °C), between 18000 s and 25200 s of self-healing (Fig. 7). In the mixtures with higher thermal inertia (M2 and M3), the optimum self-healing temperature corresponds to the lower limit of the optimum range (between 95 °C and 105 °C), outlining a joint dependence of the temperature-time variables on the degree of self-healing. The optimum temperature for these mixtures (M2 and M3) was obtained at 18000 s and 30000 s. This temperature-time dependence in the effectiveness of the self-healing process is because, in addition to achieving flow behavior in the binder, the binder must have sufficient time to drain and thermally expand through the entire crack, sealing it completely to complete the healing process.

The reference mix presented an average self-healing rate of 36.78 %, similar to the average value obtained by the M2 mix corresponding to 44.53 % with a significance of sig. = 0.157. However, the self-healing value for the M2 mix increases by 24.72 %, with a value in the healing rate of 55.54 % and a significance of sig. = 0.053 concerning the reference mix when considering only the self-healing values within the optimum range for each of the mixes. As for the M1 mixture with replacement of GA by CS at the 2 mm size, it presented the highest self-healing values of the study with a mean self-healing rate value of 52.10 %, a value that increases to 57.18 % when considering only the values of its optimum range (between 105 °C and 110 °C). This behavior could be due to the lower thermal inertia shown by this size, which contributes to a longer healing time and binder slipping through the crack, and to the higher void content presented by this mixture close to 6 % (see Table 6).

Finally, mix M3 showed the lowest values for the retained strength ratio (self-healing rate) with an average value of 44.48 % in its optimum range.

Table 7
Penetration and ring and ball test results.

Specifications	Unit	Results		
		B50/70	B50/70 Fab.	B50/70 9 h
Penetration, 25 °C	mm/10	57	25 ± 0.01	21 ± 0.01
Softening point	°C	51.6	62.7	65.7
Penetration index	-	-0.5	0.01	0.19

3.4. Binder rheological characterization

Table 7 shows the values obtained in the penetration and ring and ball tests for binders B50/70, B50/70 Fab. and B50/70 9 h. An increase in the penetration and softening temperature values for the binders after the manufacturing (B50/70 Fab.) and self-curing (B50/70 9 h) processes is observed. This behavior is due to an increase in binder stiffness after the manufacturing process, a phenomenon that will be validated with DSR test results.

Fig. 8 and Fig. 9 show the effects of temperature and the fabrication and self-healing processes at 9 h (32400 s) on the values of the complex modulus (G^*) and complex viscosity (η^*) of the B50/70 binder, respectively.

An increase in the complex modulus G^* of the binder samples extracted after manufacturing and 9 h of self-healing is observed for all the test temperatures analyzed, in comparison to binder B50/70 (see Fig. 8). This increase in binder stiffness is due to a phenomenon of aging and volatilization of its aromatic components during the fabrication processes. This increase in the stiffness of the aged binder is equivalent to a 10 °C reduction in the DSR test temperature of the B50/70 binder. A similar case occurs with the values of the complex viscosity η^* (Fig. 9) where the B50/70 Fab. and B50/70 9 h extraction binders present a higher viscoelasticity state ($> \eta^*$) than the virgin binder with a shift of the viscosity curve upwards, reflecting a higher degree of aging in these samples. No significant differences (sig. < 0.05) are observed in the complex modulus and viscosity values for the B50/70 Fab. and B50/70 9 h binder samples, showing that the self-healing process by UV radiation does not generate accelerated aging of the asphalt binder.

Fig. 10 shows the dependence of the complex viscosity η^* of the B50/70 binder on the temperature and frequency of load application. A pseudo-plastic behavior of the binder for the lowest temperatures (between 30 °C and 80 °C) with a decrease in viscosity with increasing frequency is observed. The independence of the complex viscosity from the applied shear frequency at temperatures > 90 °C is noticed, outlining an almost Newtonian behavior of the binder.

The importance of obtaining a Newtonian flow behavior of the binder in the healing and self-healing processes of asphalt mixtures is noted, based on the above mentioned and according to the higher values of self-healing rates for temperatures between 95 °C and 110 °C. Fig. 11 shows the flow behavior index (n) for B50/70, B50/70 Fab. and B50/70 9 h binders at different temperatures. Values of $0.9 \leq n < 1.0$ indicate near Newtonian behavior of the binder, while values of

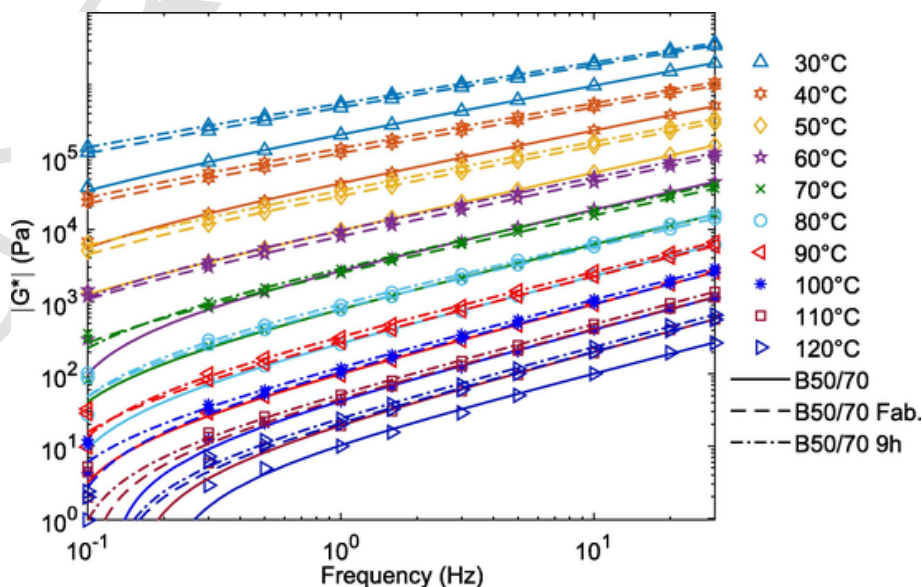


Fig. 8. Complex module, G^* .

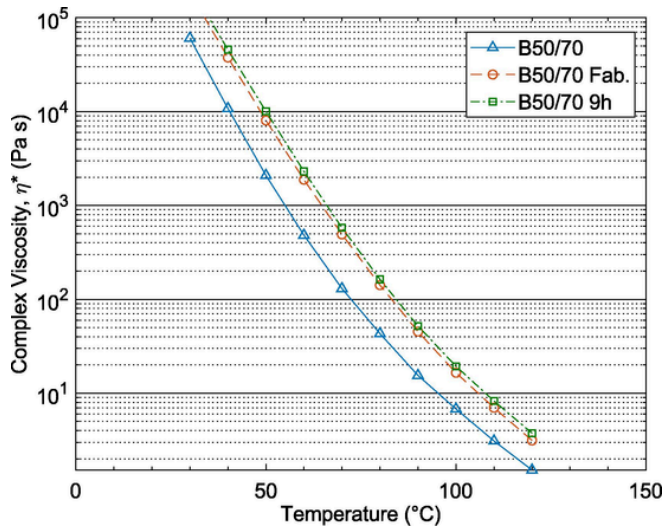


Fig. 9. Results for complex viscosity, η^* at 0.1 Hz.

$n = 1.0$ represent ideal Newtonian behavior. As expected, all samples show similar flow behavior with an increase in the value of n with temperature and values close to 1.0 at 120 °C.

The B50/70 binder starts its self-healing process (pseudonewtonian flow behavior, $n = 0.9$) at 60.25 °C, while the B50/70 Fab. and B50/70 9 h binders start at 79.38 °C and 81.82 °C, respectively. According to the above, it is again not possible to evidence an accelerated aging effect in the mixtures after the 9 h healing processes (32400 s) with flow temperature differences of $<3\%$, which would allow several self-healing cycles to be performed without modifying the rheological properties of the binder.

4. Conclusions

Based on the results obtained and the statistical tests carried out in the study of UV self-healing of semi-dense asphalt mixes incorporating

different sizes of copper slag (CS) in partial replacement of natural aggregate (AG), the following conclusions can be drawn:

- The mixes incorporating the smaller CS sizes showed higher thermal inertia than the conventional mix, slowing down the temperature increase on their surface. This phenomenon decreases with increasing CS size, with the 2.00 mm CS replacement having similar thermal inertia to conventional mix.
- The mixtures with the highest thermal inertia reached a steady-state temperature between 108 °C and 110 °C. Whereas, in the mixtures with lower thermal inertia, it was not possible to visualize a temperature steady-state condition.
- All mixtures incorporating CS achieved an average self-healing rate of more than 30 %. This value increases to an average self-healing rate of over 40 % when considering only those mixtures that reached the optimum self-healing temperatures.
- The mixture with 2.00 mm size replacement of CS by AG showed the highest degree of self-healing with healing rate values of up to 71.69 % with an optimum mean of 57.18 %. The reference mixtures did not exceed 60 % in self-healing rate with a mean of 36.78 %.
- The optimum self-healing temperatures are between 95 °C and 105 °C for the higher thermal inertia mixes (mixtures with CS of 0.25 mm and CS <0.063 mm) and between 105 °C and 110 °C for the lower thermal inertia mixes (mixtures with 2.00 mm CS and conventional mixture). Temperatures above 110 °C cause a significant decrease in the self-healing rate of asphalt mixes.
- Temperatures of 95 °C and 110 °C were reached in almost all the times considered in this study, validating these times as optimal self-healing periods for UV radiation in asphalt mixes. The optimum self-healing period for the mixtures with lower thermal inertia is obtained between 18000 s and 25200 s, while that of the mixtures with higher thermal inertia is obtained for times from 18000 s to 30000 s.
- It was not possible to determine an accelerated aging effect on the asphalt mixtures by the self-healing and UV radiation processes, because no significant differences in the values of complex

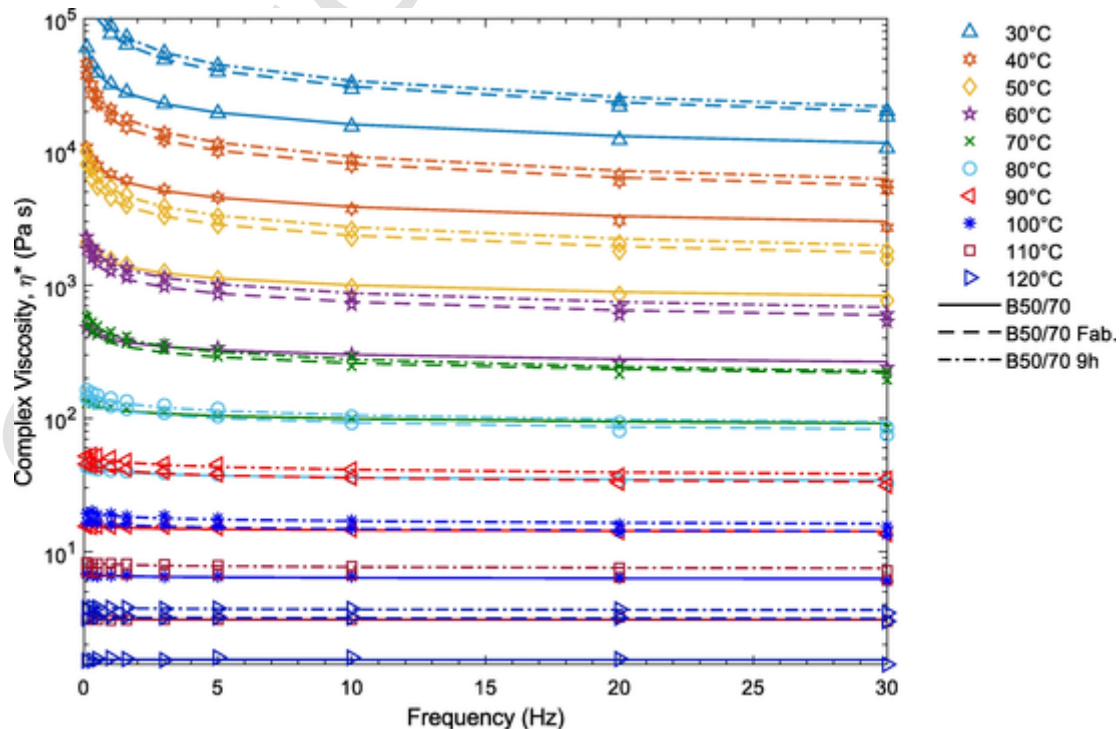


Fig. 10. Results of complex viscosity, η^* of binder B50/70, after fabrication process (B50/70 Fab.) and after 9 h self-healing process (B50/70 9 h).

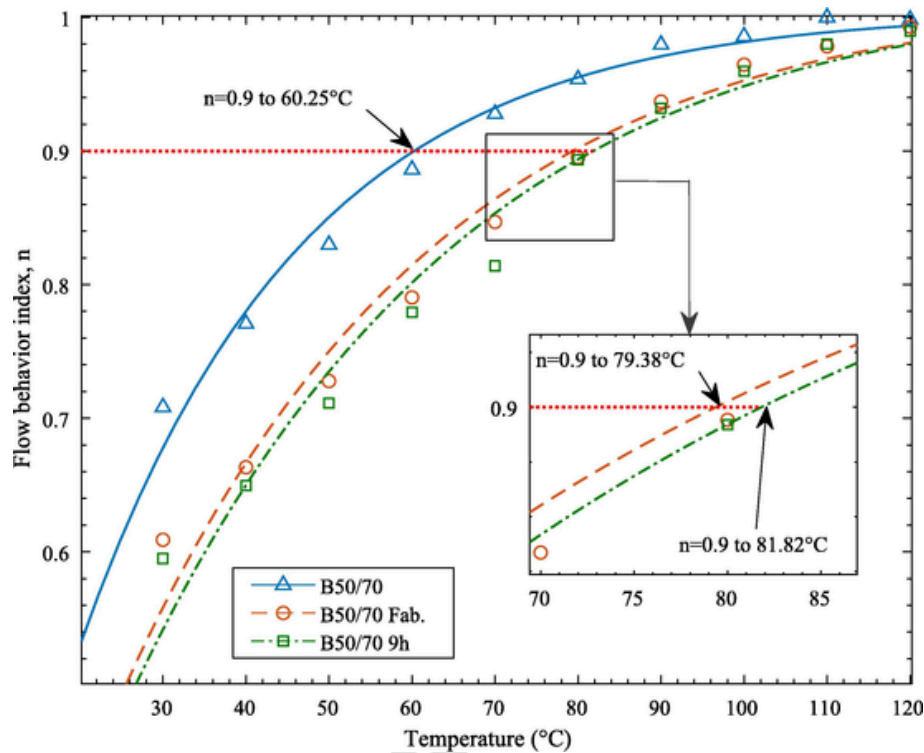


Fig. 11. Flow behavior index (n) at 0.1 Hz of B50/70, B50/70 Fab. and B50/70 9 h binders.

modulus and viscosity were observed in comparison to the binder extracted after fabrication.

- The self-healing processes did not change the flow behavior of the B50/70 asphalt binder, which would allow several self-healing processes to be carried out under the same temperature conditions as the first self-healing process.

In general, the results obtained showed that CS of larger sizes presents a good performance in the self-healing of asphalt mixtures by UV radiation. Future research should study the elastic properties of self-healing asphalt mixtures, as well as the variation in the self-healing rate after several curing cycles.

Declaration of Competing Interest

The authors declare that they have no known competing financial interests or personal relationships that could have appeared to influence the work reported in this paper.

Acknowledgments

The authors are grateful for the institutional support provided by the Vice-Rector for Research, Development and Artistic Creation (VIDCA UACH) and the InnovING 2030 project of the Faculty of Engineering Sciences UACH. The authors would also like to thank the GITECO Research Group of the University of Cantabria and its technical staff for their support in the development of the laboratory tests.

Funding

This work was funded by the National Research and Development Agency of Chile ANID/CONICYT through the FONDECYT Regular Research program [1211160].

References

- [1] G. Liu, T. Yang, J. Li, Y. Jia, Y. Zhao, J. Zhang, Effects of aging on rheological properties of asphalt materials and asphalt-filler interaction ability, *Constr. Build. Mater.* 168 (2018) 501–511, <https://doi.org/10.1016/j.conbuildmat.2018.02.171>.
- [2] R. Delgado, C. Wahr, G. García, A. González. Asphalt technology in Chile: Leading research and practice, in: *Asph. Paving Technol.* AAPT. 2012.
- [3] P. Cui, S. Wu, Y. Xiao, C. Yang, F. Wang, Enhancement mechanism of skid resistance in preventive maintenance of asphalt pavement by steel slag based on micro-surfacing, *Constr. Build. Mater.* 239 (2020) 117870, <https://doi.org/10.1016/j.conbuildmat.2019.117870>.
- [4] J.C. Petersen, A Review of the Fundamentals of Asphalt Oxidation (E-C140), *Transp. Res. Rec. J. Transp. Res. Board. E-C 140* (2009) 1–78.
- [5] A.A.A. Molenaar, E.T. Hagos, M.F.C. van de Ven, Effects of aging on the mechanical characteristics of bituminous binders in PAC, *J. Mater. Civ. Eng.* 22 (2010) 779–787, [https://doi.org/10.1061/\(ASCE\)MT.1943-5533.0000021](https://doi.org/10.1061/(ASCE)MT.1943-5533.0000021).
- [6] K.H.I.A. Helo, Z.I. Qasim, M.A. Abdulhusein, Effect of laboratory aging on moisture susceptibility of polymer-modified bituminous mixtures, *IOP Conf. Ser.: Mater. Sci. Eng.* 737 (1) (2020) 012131.
- [7] A.E. Hidalgo, F. Moreno-Navarro, R. Tauste, M.C. Rubio-Gámez, The Influence of Reclaimed Asphalt Pavement on the Mechanical Performance of Bituminous Mixtures, *An Analysis at the Mortar Scale, Sustain.* 12 (20) (2020) 8343.
- [8] J. Qiu, M.V. de Ven, A. Molenaar, Crack-healing investigation in bituminous materials, *J. Mater. Civ. Eng.* 25 (2013) 864–870, [https://doi.org/10.1061/\(ASCE\)MT.1943-5533.0000744](https://doi.org/10.1061/(ASCE)MT.1943-5533.0000744).
- [9] L. Ann Myers, R. Roque, B.E. Ruth, C. Drakos, Measurement of Contact Stresses for Different Truck Tire Types To Evaluate Their Influence on Near-Surface Cracking and Rutting, *Transportation Research Record* 1655 (1) (1999) 175–184.
- [10] B. Birgisson, A. Montepara, E. Romeo, R. Roncella, J.A.L. Napier, G. Tebaldi, Determination and prediction of crack patterns in hot mix asphalt (HMA) mixtures, *Eng. Fract. Mech.* 75 (2008) 664–673, <https://doi.org/10.1016/j.engfracmech.2007.02.003>.
- [11] V. Kumar V, S. Saride, Use of Digital Image Correlation for the Evaluation of Flexural Fatigue Behavior of Asphalt Beams with Geosynthetic Interlayers, *Transportation Research Record* 2631 (1) (2017) 55–64.
- [12] S. Xu, A. García, J. Su, Q. Liu, A. Tabaković, E. Schlangen, Self-Healing Asphalt Review: From Idea to Practice, *Adv. Mater. Interfaces.* 5 (2018), <https://doi.org/10.1002/admi.201800536>.
- [13] G. Mazzoni, A. Stimilli, F. Canestrari, Self-healing capability and thixotropy of bituminous mastics, *Int. J. Fatigue.* 92 (2016) 8–17, <https://doi.org/10.1016/j.ijfatigue.2016.06.028>.
- [14] A. Tabaković, E. Schlangen, Self-healing technology for asphalt pavements, *Adv. Polym. Sci.* (2016), https://doi.org/10.1007/12_2015_335.
- [15] Á. García, E. Schlangen, M. van de Ven, Q. Liu, Electrical conductivity of asphalt mortar containing conductive fibers and fillers, *Constr. Build. Mater.* 23 (2009) 3175–3181, <https://doi.org/10.1016/j.conbuildmat.2009.06.014>.

- [16] J. Norambuena-Contreras, A. Garcia, Self-healing of asphalt mixture by microwave and induction heating, *Mater. Des.* 106 (2016) 404–414, <https://doi.org/10.1016/j.matdes.2016.05.095>.
- [17] J. Gallego, M.A. Del Val, V. Contreras, A. Páez, Heating asphalt mixtures with microwaves to promote self-healing, *Constr. Build. Mater.* 42 (2013) 1–4, <https://doi.org/10.1016/j.conbuildmat.2012.12.007>.
- [18] H. Ajam, P. Lastra-González, B. Gómez-Mejide, G. Airey, A. Garcia, Self-Healing of Dense Asphalt Concrete by Two Different Approaches: Electromagnetic Induction and Infrared Radiation, *J. Test. Eval.* 45 (2017) 20160612, <https://doi.org/10.1520/JTE20160612>.
- [19] A. García, E. Schlangen, M. van de Ven, Two Ways of Closing Cracks on Asphalt Concrete Pavements: Microcapsules and Induction Heating, *Key Eng. Mater.* 417–418 (2009) 573–576, <https://doi.org/10.4028/www.scientific.net/KEM.417-418.573>.
- [20] A. García, M. Bueno, J. Norambuena-Contreras, M.N. Partl, Induction healing of dense asphalt concrete, *Constr. Build. Mater.* 49 (2013) 1–7, <https://doi.org/10.1016/j.conbuildmat.2013.07.105>.
- [21] J. Tang, Q. Liu, S. Wu, Q. Ye, Y. Sun, E. Schlangen, Investigation of the optimal self-healing temperatures and healing time of asphalt binders, *Constr. Build. Mater.* 113 (2016) 1029–1033, <https://doi.org/10.1016/j.conbuildmat.2016.03.145>.
- [22] D.M. Heyes, P.J. Mitchell, P.B. Visscher, Viscoelasticity and near-newtonian behaviour of concentrated dispersions by Brownian dynamics simulations BT – Trends in Colloid and Interface Science VIII, in: R.H. Ottewill, A.R. Rennie (Eds.), *Progress in Colloid & Polymer Science/Trends in Colloid and interface Science VIII*, Steinkopff, Darmstadt, 1994, pp. 179–182.
- [23] F. Moreno-Navarro, M. Sol-Sánchez, A. Jiménez del Barco, M.C. Rubio-Gámez, Analysis of the influence of binder properties on the mechanical response of bituminous mixtures, *Int. J. Pavement Eng.* 18 (2017) 73–82, <https://doi.org/10.1080/10298436.2015.1057138>.
- [24] J.F. Su, J. Qiu, E. Schlangen, Y.Y. Wang, Investigation the possibility of a new approach of using microcapsules containing waste cooking oil: In situ rejuvenation for aged bitumen, *Constr. Build. Mater.* 74 (2015) 83–92, <https://doi.org/10.1016/j.conbuildmat.2014.10.018>.
- [25] T. Al-Mansoori, R. Micaelo, I. Artamendi, J. Norambuena-Contreras, A. Garcia, Microcapsules for self-healing of asphalt mixture without compromising mechanical performance, *Constr. Build. Mater.* 155 (2017) 1091–1100, <https://doi.org/10.1016/j.conbuildmat.2017.08.137>.
- [26] A. Garcia, C.J. Austin, J. Jelfs, Mechanical properties of asphalt mixture containing sunflower oil capsules, *J. Clean. Prod.* 118 (2016) 124–132, <https://doi.org/10.1016/j.jclepro.2016.01.072>.
- [27] A. García, J. Norambuena-Contreras, M. Bueno, M.N. Partl, Influence of steel wool fibers on the mechanical, thermal, and healing properties of dense asphalt concrete, *J. Test. Eval.* 42 (5) (2014) 20130197.
- [28] A. Garcia, S. Salih, B. Gómez-Mejide, Optimum moment to heal cracks in asphalt roads by means electromagnetic induction, *Constr. Build. Mater.* 238 (2020) 117627.
- [29] J. Liu, T. Zhang, H. Guo, Z. Wang, X. Wang, Evaluation of self-healing properties of asphalt mixture containing steel slag under microwave heating: Mechanical, thermal transfer and voids microstructural characteristics, *J. Clean. Prod.* 342 (2022) 130932.
- [30] Y.H. Sun, Q.T. Liu, S.P. Wu, F. Shang, Microwave Heating of Steel Slag Asphalt Mixture, *Microwave heating of steel slag asphalt mixture* 599 (2014) 193–197.
- [31] B.H. Dinh, D.W. Park, T.M. Phan, Healing Performance of Granite and Steel Slag Asphalt Mixtures Modified with Steel Wool Fibers, *KSCE J. Civ. Eng.* 22 (2018) 2064–2072, <https://doi.org/10.1007/S12205-018-1660-8>.
- [32] X. Zhu, F. Ye, Y. Cai, B. Birgisson, K. Lee, Self-healing properties of ferrite-filled open-graded friction course (OGFC) asphalt mixture after moisture damage, *J. Clean. Prod.* 232 (2019) 518–530, <https://doi.org/10.1016/J.JCLEPRO.2019.05.353>.
- [33] B. Gómez-Mejide, H. Ajam, P. Lastra-González, A. Garcia, Effect of air voids content on asphalt self-healing via induction and infrared heating, *Constr. Build. Mater.* 126 (2016) 957–966, <https://doi.org/10.1016/J.CONBUILDMAT.2016.09.115>.
- [34] S. Shirzad, M.M. Hassan, M.A. Aguirre, L.N. Mohammad, S. Cooper, I.I. Negulesco, Mechanical and Self-Healing Performances of Asphalt Mixtures Containing Recycled Asphalt Materials and Light-Activated Self-Healing Polymer, *J. Mater. Civ. Eng.* 31 (11) (2019), [https://doi.org/10.1061/\(ASCE\)MT.1943-5533.0002903](https://doi.org/10.1061/(ASCE)MT.1943-5533.0002903).
- [35] A.C. Raposeiras, D. Movilla-Quesada, O. Muñoz-Cáceres, V.C. Andrés-Valeri, M. Lagos-Varas, Production of asphalt mixes with copper industry wastes: Use of copper slag as raw material replacement, *J. Environ. Manage.* 293 (2021) 112867.
- [36] S.N. de G. y Minería, Anuario de la minería de Chile 2018, 2018.
- [37] A.C. Raposeiras, D. Movilla-Quesada, R. Bilbao-Novoa, C. Cifuentes, G. Ferrer-Norambuena, D. Castro-Fresno, The use of copper slags as an aggregate replacement in asphalt mixes with RAP: Physical–chemical and mechanical behavioural analysis, *Constr. Build. Mater.* 190 (2018) 427–438, <https://doi.org/10.1016/j.conbuildmat.2018.09.120>.
- [38] O. Muñoz-Cáceres, A.C. Raposeiras, D. Movilla-Quesada, D. Castro-Fresno, M. Lagos-Varas, V.C. Andrés-Valeri, G. Valdés-Vidal, Mechanical performance of sustainable asphalt mixtures manufactured with copper slag and high percentages of reclaimed asphalt pavement, *Constr. Build. Mater.* 304 (2021) 124653, <https://doi.org/10.1016/j.conbuildmat.2021.124653>.
- [39] E.T. Harrigan, R.B. Leahy, J.S. Youtcheff, S.H.R. Program, C.A. National Research Council NW, D.C. 20418 U.S.A. Washington, Superpave manual of specifications, test methods and practices, SHRP-A-379, Strategic Highway Research Program, National Research Council, Washington, DC, Washington, DC., 1994.
- [40] J. Chen, T. Pan, X. Huang, Numerical investigation into the stiffness anisotropy of asphalt concrete from a microstructural perspective, *Constr. Build. Mater.* 25 (2011) 3059–3065, <https://doi.org/10.1016/j.conbuildmat.2011.01.002>.
- [41] D. Movilla-Quesada, O. Muñoz, A.C. Raposeiras, D. Castro-Fresno, Thermal susceptibility analysis of the reuse of fly ash from cellulose industry as contribution filler in bituminous mixtures, *Constr. Build. Mater.* 160 (2018) 268–277.
- [42] A. Ala, C.C. Baek, M. Eyad, P. Tom, The influence of laboratory aging method on the rheological properties of Asphalt binders, *J. Test. Eval.* 30 (2002) 171–176. <http://cat.inist.fr/?aModele=afficheN&cpsidt=13571974>.
- [43] F. Moreno-Navarro, M. Sol, M.C. Rubio-Gámez, A. Ramírez, Reuse of thermal power plant slag in hot bituminous mixes, *Constr. Build. Mater.* 49 (2013) 144–150, <https://doi.org/10.1016/j.conbuildmat.2013.07.090>.
- [44] M. Vila-Cortavitarte, D. Jato-Espino, D. Castro-Fresno, M. Calzada-Pérez, Self-healing capacity of asphalt mixtures including by-products both as aggregates and heating inductors, *Materials (Basel)*. 11 (5) (2018) 800.
- [45] X. Lu, U. Isacson, Effect of ageing on bitumen chemistry and rheology, *Constr. Build. Mater.* 16 (2002) 15–22, [https://doi.org/10.1016/S0950-0618\(01\)00033-2](https://doi.org/10.1016/S0950-0618(01)00033-2).
- [46] H. Ziari, A. Moniri, R. Imaninasab, M. Nakhaei, Effect of copper slag on performance of warm mix asphalt, *Int. J. Pavement Eng.* 20 (2019) 775–781, <https://doi.org/10.1080/10298436.2017.1339884>.
- [47] Y.K. Tandel, J.B. Patel, Review of utilisation of copper slag in highway construction, *Aust. Geomech. J.* 44 (2009) 71–80.
- [48] A.M. Zaltoum, A review study of the effect of air voids on asphalt pavement life, (2018).